Introduction to Energy Harvesting Transducers and Their Power Conditioning Circuits

Baoxing Chen

1 Introduction

Wireless sensor nodes are usually powered by batteries; however, maintenance for them can become a significant hassle. Batteries have limited life span and they need to be replaced. In some applications, the wireless sensor nodes can be installed in a remote and tough-to-reach area. Maintenance-free wireless sensor nodes are essential to drive the continuous adoption of wireless sensor network for wide range of IoT applications, from machine health monitoring, building automation, to smart wearables. Energy harvesting, i.e., harvesting energy from the ambient environment, is an ideal solution to enable maintenance-free wireless sensor network. An energy harvesting system for wireless sensors consists of the following as shown in Fig. 1.: (1) one or multiple energy harvesters; (2) some kind of energy storage device; (3) power management device to ensure efficient energy extraction from the harvesters, to produce the output voltages suitable for use by other devices, and to manage the storage device; (4) various sensors to sense a variety of environmental data such as temperature, pressure, or gas; (5) the signal conditioning circuits and microcontrollers to interface with the sensors,; and (6) the wireless transceivers. In this chapter, we will mainly focus on 1, 2, and 3.

B. Chen (✉)
Analog Devices, Inc., Wilmington, MA, USA
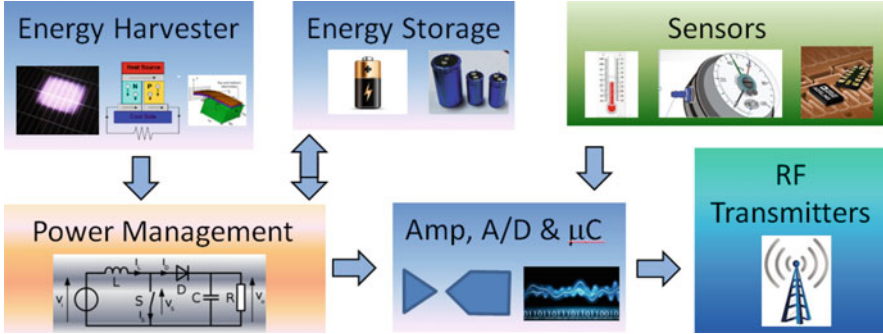e-mail: Baoxing.Chen@analog.com
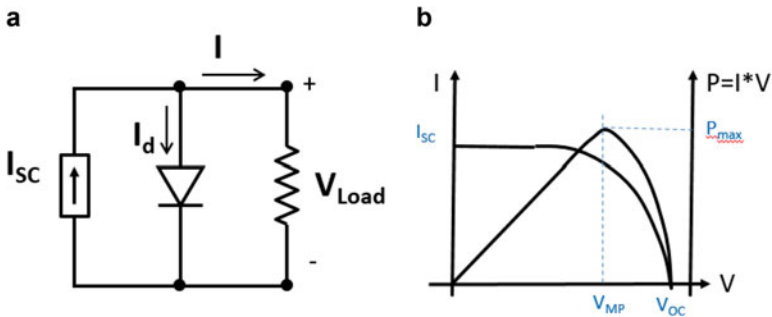
Fig. 1 Typical energy harvesting system

Fig. 2 (**a**) Circuit model and (**b**) I-V curve for photovoltaic cell

2 Photovoltaic Harvesting

PV panels can usually generate around 100 W/m^2 or 10 mW/cm^2 outdoors with 10% solar cell efficiency, but this number can drop 2–3 orders of magnitude indoors dependent on lighting condition. For area-constraint application, the solar cell efficiency is key. Low solar cell efficiency is due to low quantum efficiency where only the photons with energy bigger than the bandgap can be absorbed and excessive photon energy above the bandgap is also lost to heat. The solar cell efficiency can be improved with multi-junction device, where junctions with different bandgaps are stacked so that photons with different energy are absorbed more efficiently by different junctions.

Figure 2a shows the circuit model for a PV cell where the current through the load is the short circuit current minus the diode current. Figure 2b shows typical I-V curve where V_{OC} is the open circuit voltage and I$_{SC}$ is the short circuit current. The power it generates has a peak at certainly voltage V_{MP}, fraction of the V_{OC}, and this is the maximum power point with P_{max}. For the PV power conditioning circuit, it is important that solar cell operates at this point. With low power application, we need to balance the power gain from the additional efficiency gain from accurate
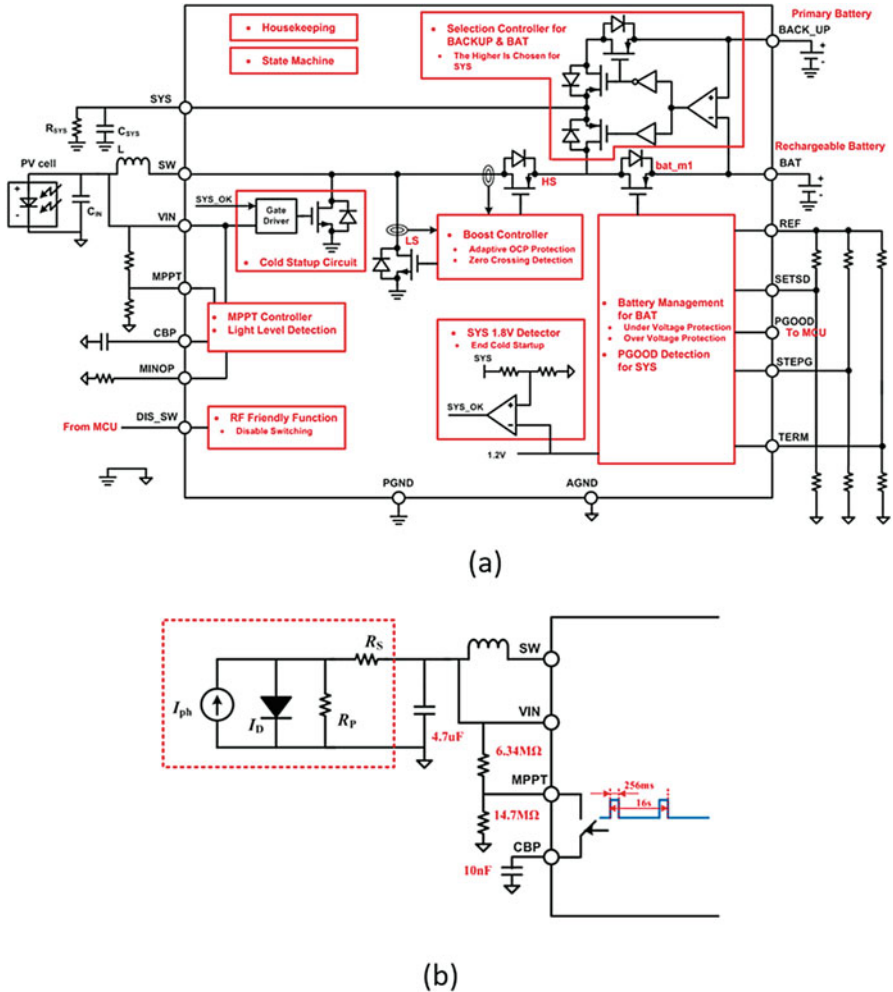
Fig. 3 (**a**) Boost converter architecture (ADP5090) and (**b**) VOC sense implementation

maximum power point tracking and the power loss for implementing the MPPT algorithms. One common approach is to approximate the point using some fraction of the open circuit voltage (FOV). While the V_{OC} changes with different lighting conditions, FOV stays relatively constant. This can be easily implemented with a comparator and voltage divider. The load can be either disrupted to get V_{OC} or a dummy reference cell is used to get V_{OC}.

An example implementation for how V_{OC} is sampled is shown in Fig. 3 [1]. Figure 3a is the overall circuit architecture for an ultralow power boost converter, and Fig. 3b shows the V_{OC} sampling method. In every 16 s, the converter is interrupted for 256 mS to allow FOV to be sampled and stored in C_{BP} through a

Fig. 4 Cold startup circuit implementation

Table 1 Comparison for startup voltage and low load efficiency

Supplier features	ADI ADP5090	TI bq25504	Linear Tech LTC3105	Maxim Max17710
Start-up input voltage	380 mV	330 mV	ZSOmV	750 mV
Efficiency (Vin@0.5 V; Vout@3.0 V)	58% (10 uA) 79% (100 uA)	35% (10 uA) 75% (100 uA)	30% (10 uA) 50% (100 uA)	Not supported
lq	≈350 nA	570 nA	10 uA	625 nA

voltage divider of V_{OC}. Since a single cell output voltage can be low, an important piece of the PV harvesting is the cold startup circuit. An example implementation is shown in Fig. 4 [2].

The first charge pump 10*VIN_CP is used to control a cascade device to protect the 3 V medium VT startup switch MV from the switching node voltages, and a comparator is used to make sure the second charge pump output voltage 4*VIN_CP is good. Inductor current saturation is detected to minimize startup current as long startup period from a regular oscillator can easily make inductor current saturated. Table 1 is the summary of startup voltage and efficiencies for a few ultralow power boost converters on the market. As much as 58% efficiency can be achieved with only 10uA load, and the quiescent current is only about 350 nA.

3   Thermoelectric Harvesting

Thermoelectric harvesters rely on a temperature gradient to generate power based on one of the thermoelectric effects, the Seeback effect, which is the direct conversion of temperature differences to electric voltages. The efficiency for a thermoelectric

generator depends not only on the temperatures at the hot side and cold side but also on the figure of merit ZT for the thermoelectric material used, where $ZT = \frac{S^2 \sigma T}{\kappa}$. S is the Seeback coefficient or the thermopower, σ is the electrical conductivity, and κ is the thermal conductivity. The best bulk thermoelectric material at room temperature is Bi_2Te_3, which has a ZT ~ 1. Besides materials, there has been progress in enhancing ZT using low-dimensional structures such as quantum wells or nano-wires where larger S and/or lower thermal conductivity can be achieved.

Thermoelectric harvesters are scalable and are suitable for integration. The efficiency of a thermoelectric element does not depend on the size, and the heat that can conduct through a certain cross-section area for a given thermoelectric element increases with the reduction in its length. However, the reduction in length will lead to reduction in thermal resistance which can pose challenges in applications with high external thermal resistances where the available temperature gradient is divided between external and internal thermal resistances and only the gradient across the thermoelectric element contributes to the power generation. A thermoelectric harvester usually consists of multiple thermoelectric legs with positive thermoelectric power (p-type) and negative thermoelectric power (n-type) connected in series electrically, but in parallel thermally, to build enough voltage that can be used. The voltage across a single element can be quite small, and in many cases, a booster converter is used to further raise the voltage and ensures impedance matching to extract the maximum power from the harvester. To reduce the thermal shunt by the ambient air surrounding the P and N legs, wafer capping can be used to seal the thermoelectric legs in a vacuum as shown in Fig. 5a [3]. To improve device thermal resistance without the need for thick films, the thermoelectric films can be deposited along a thick polyimide island as shown in Fig. 5b.

A thermoelectric harvester delivers the maximum power to the load when the load resistance matches the internal device resistance. Similar circuit can be adapted from FOV for the PV cell harvesting but setting FOV equal to 0.5. Besides load matching for maximum power, another common need is the startup circuit due to the low voltage output from the thermoelectric harvester with limited DT. Depleted NMOS together with a step-up transformer can form self-oscillation to build up
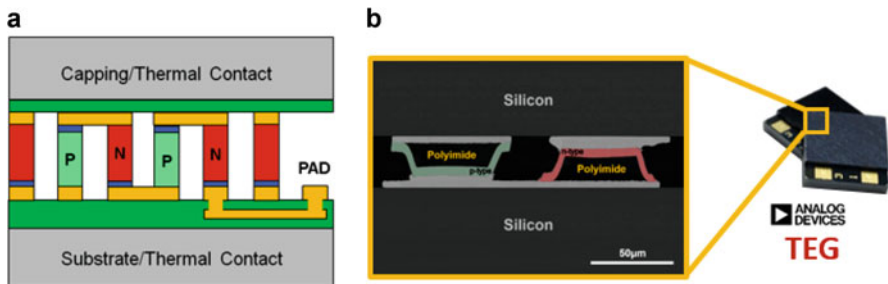

Fig. 5 (**a**) Structure for a vertical thermoelectric harvester with vacuum capping (**b**) pyramid-shaped thermoelectric harvester
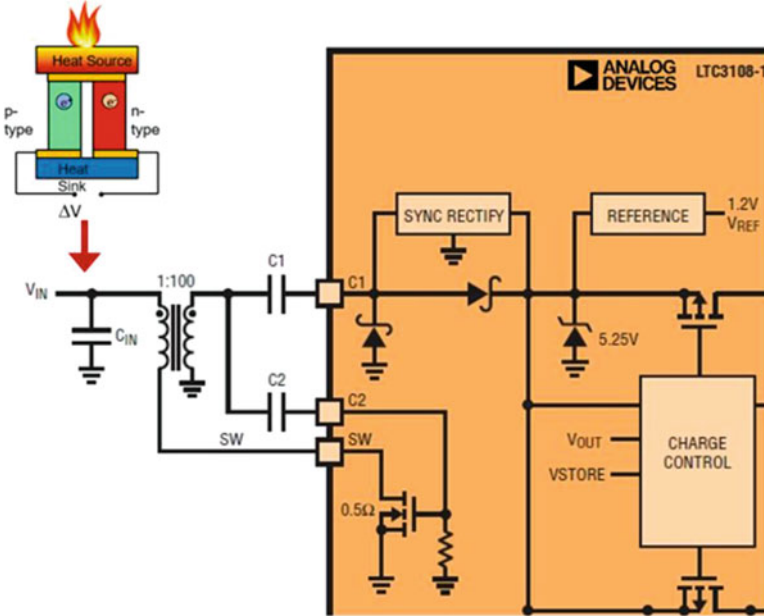
Fig. 6 Low voltage startup using step-up transformers

startup voltage as shown in Fig. 6 [4]. With 1:100 step-up transformers, the converter can startup from input as low as 20 mV. In some applications, the harvester also needs to harvest energy from both positive input voltages and negative input voltages. For example, a ground spike can be used to harvest energy from the temperature differences between the surface and the soil under, and the polarity can change depending on the day or night. A full bridge circuit with parallel diodes and switches can be used, and the switches are turned on or off by looking at the voltage polarities at the input. For bipolar startup, two startup transformers can be used [5].

4 Vibrational Harvesting

Vibrational harvesters usually rely on certain mechanical structures to convert external vibration to the kinetic energy, and the mechanical structures are coupled to energy transducers, such as piezoelectric transducers or electromagnetic transducers, to convert kinetic energy to electricity. Figure 7a shows a typical cantilever-based piezoelectric harvester. The beam operates in a bending mode, strains the piezoelectric films, and generates charges from the piezoelectric effect. While a cantilever provides low resonant frequency, a proof mass at the end further reduces the resonant frequency, more suitable for low-frequency vibrational
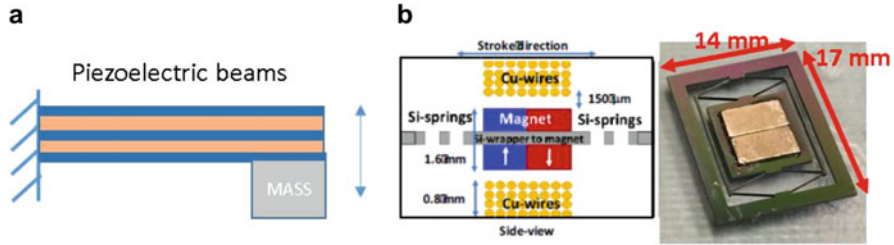
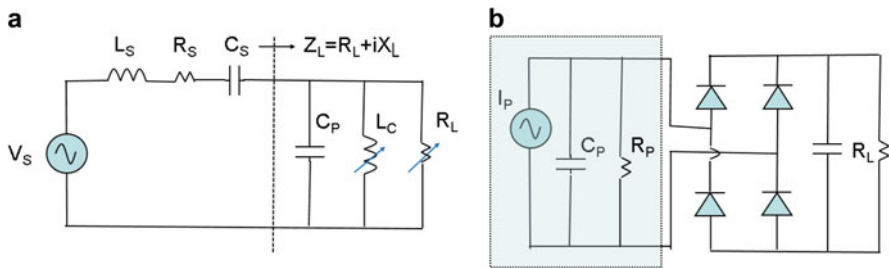**Fig. 7** (**a**) Piezoelectric harvester (**b**) electromagnetic harvester

Fig. 8 (**a**) Piezoelectric harvester model (**b**) full bridge rectifier for the harvester

harvesting. Figure 7b shows an example MEMS electromagnetic harvester [6]. The magnets mount on a silicon spring, and the magnetic field will cut across the coils mount above and below the magnet once the spring oscillates. Vibrational harvesters can be analyzed using damped mass-spring systems [7]. It is desired to maximize the mass displacement with the power increasing with the square of the amplitude but the mass displacement is limited by the size of the system.

Equivalent circuit model for a piezoelectric harvester is shown in Fig. 8a. Its source impedance is equivalently a serial RLC network [8], where $RS = \eta/\Theta^2$, $LS = M/\Theta^2$, $CS = \Theta^2/K$. η is the mechanical damping coefficient, Θ is the piezoelectric coefficient, M is the mass, and K is the effective stiffness. This can be derived from the vibration and transducing equations. The dotted line represents electromechanical interface. To extract maximum power into the electrical domain, it is desired that the loading impedance $Z_L = R_L + jX_L$ be the complex conjugate of the source impedance, $Z_S^* = R_S - jX_S$, where $X_S = \omega L_S - 1/(\omega C_S)$. With conjugate matching, the source basically sees source impedance R_S and R_L, and current and voltage waveforms are synchronized. In principle, Z_L can be adjusted with variable L_C and R_L but L_C can be large, tens to hundreds of Henry. In many practical systems, simple full bridge rectifier is used without conjugate matching as shown in Fig. 8b; however, the efficiency can be low as its ideal efficiency is only $4/\pi Q_P$, where $Q_P = \omega_P C_P R_P$ and Q_P is usually bigger than 10. Its efficiency can be improved to $8/\pi Q_P$ with a bias flip switch without inductors, and the harvesting efficiency can be dramatically boosted with synchronized switching harvesting on
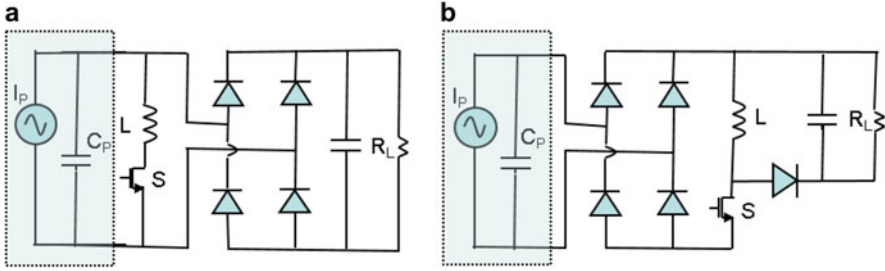
Fig. 9 (**a**) SSHI diagram (**b**) SECE diagram

inductors (SSHI) [9, 10] or synchronous electrical charge extraction (SECE) [11] as shown in Fig. 9.

SSHI adds an inductive switch path, *L* and *S*, to avoid the energy wasted for charging and discharging internal capacitance C_P. SECE has a switch *S* that will turn on each time the rectified voltage reaches maximum and turn off each time it reaches 0. This allows the stored charge to be removed completely and for the transducer to deliver the power to the load through L. Full wave rectified diodes, as shown in Fig. 9, can lead to significant rectification loss with the finite diode drop. Active NMOS with cross-coupled PMOS or active PMOS with cross-coupled NMOS can be used to reduce rectification loss considerably. With limited harvested energy, the comparators used to control the active switches need to be designed with low quiescent power.

While synchronized switching can boost harvester efficiency, it relies on the harvesters operating at resonant frequencies. However, the manufactured harvesters can have certain percentage of variations in their resonant frequencies because of manufacturing tolerances, and extracted power can be significantly lower if these resonant frequencies do not match those of the vibrational sources. Off-resonance efficiency can be improved by introducing switching delays for synchronized switching techniques based on the conjugate impedance matching principle [12].

As shown in Fig. 10a, synchronized switching can be analyzed with a simple current source with parallel capacitance in parallel with a serial-connected inductor and switches. At zero crossing of the source current, the switch turns on for half of the period of the LC resonance to allow V_S to be flipped. V_S is not an ideal square waveform with the loss in switches and inductors. Similarly, the synchronized switching waveforms with delays can be shown in Fig. 11. If the delay is positive, the load appears capacitive as shown in Fig. 11a, and if the delay is negative, the load appears inductive as shown in Fig. 11b. A delay to the voltage waveform basically introduces a quadrature term besides the fundamental term. The equivalent impedance seen at the electromechanical interface becomes complex. By adjusting the delay, the equivalent complex impedance can be tuned to match the conjugate source impedance for maximum power transfer.
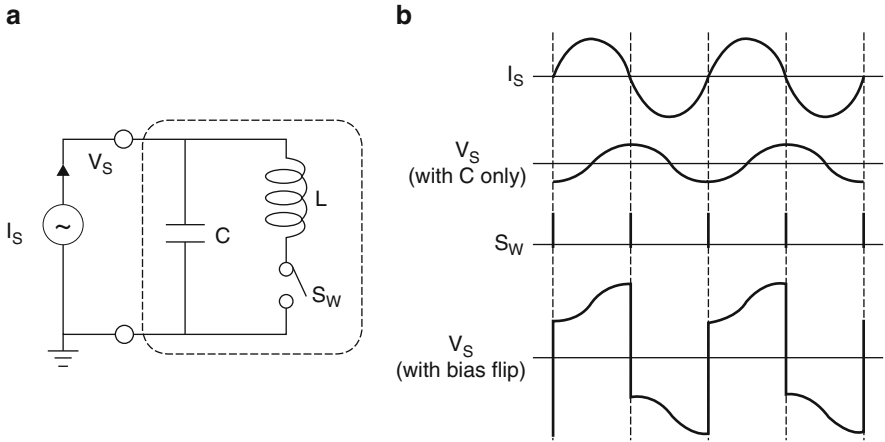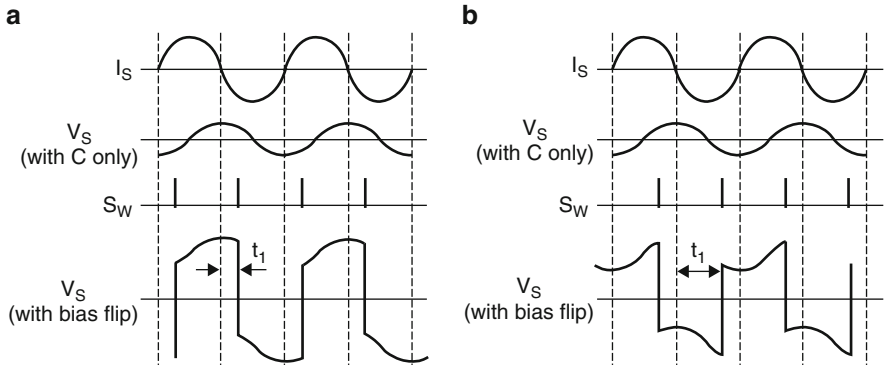
Fig. 10 (**a**) Synchronized switching schematic (**b**) waveforms

Fig. 11 Synchronized switching with (**a**) positive delay (**b**) negative delay

5   Conclusions

Various energy harvesting transducers and their power conditioning circuits have been reviewed and discussed. Both the transducers and power conditioning circuits need to be optimized to maximize the power delivered to the load. While nonlinear harvesting circuits such as SSHI and SECE can significantly boost the output available to the load, it is important to minimize the circuit overhead for implementing these techniques. To accommodate manufacturing tolerances of the resonant frequencies for the vibrational harvester, off resonance output power can be improved through conjugate impedance matching or through introducing delays in synchronized switching.

References

1. ADP5090 datasheet. http://www.analog.com/media/en/technical-documentation/data-sheets/ADP5090.pdf.
2. Lu Y, Yao S, Shao B, Brokaw P. A 200nA single inductor dual-input-triple-output (DITO) converter with two-stage charging and process-limit cold-start voltage for photovoltaic and thermoelectric energy harvesting. ISSCC Dig. Tech. Papers, Feb. 2016, pp 368–70.
3. Cornett J, Lane B, Dunham M, Asheghi M, Goodson K, Gao Y, Sun N, Chen B. Chip-scale thermal energy harvester using Bi_2Te_3. IECON 2015-Yokahama, 41st Annual Conference of the IEEE Industrial Electronics Society, 2015, pp. 3326–9.
4. LTC3108 datasheet. http://www.linear.com/product/LTC3108.
5. LTC3109 datasheet. http://www.linear.com/product/LTC3109.
6. Shin A, Radhakrishna U, Yang Y, Zhang Q, Gu L, Riehl P, Chandrakasan AP, Lang JH. A MEMS magnetic-based vibration energy harvester. Power MEMS Proceedings, 2017, pp. 363–6.
7. Beeby S, Tudor M, White N. Energy harvesting vibration sources for microsystems applications. Meas Sci Technol. 2006;17:175–95.
8. Lien IC, Shu YC, Wu WJ, Shiu SM, Lin HC. Revisit of series-SSHI with comparison to other interface circuits in piezoelectric energy harvesting. Smart Mater Struct. 2010;19:125009–20.
9. Guyomar D, Badel A, Lefeuvre E, Richard C. Toward energy harvesting using active materials and conversion improvement by nonlinear processing. IEEE Trans Ultrason Ferroelectr Freq Control. 2005;52(4):584–95.
10. Ramadass Y, Chandraksan A. An efficient piezoelectric energy harvesting interface circuit using a bias-flip rectifier and shared inductor. IEEE J Solid State Circuits. 2010;45(1):189–204.
11. Lefeuvre E, Badel A, Richard C, Guyomar D. Piezoelectric energy harvesting device optimization by synchronous electric charge extraction. J Intell Mater Syst Struct. 2005;16(10):865–76.
12. Hsieh P-H, Chen C-H, Chen H-C. Improving the scavenged power of nonlinear piezoelectric energy harvesting interface at off-resonance by introducing switching delay. IEEE Trans Power Electron. 2015;30(6):3142–55.